# Selective Doping of Block Copolymer Nanodomains by Sputter Deposition of Iron

Mottakin M. Abul Kashem,*,[†,‡] Gunar Kaune,[†,§] Alexander Diethert,[†] Weinan Wang,[†] Kai Schlage,[‡] Sebastien Couet,[‡,⊥] Ralf Röhlsberger,[‡] Stephan V. Roth,[‡] and Peter Müller-Buschbaum*,[†]
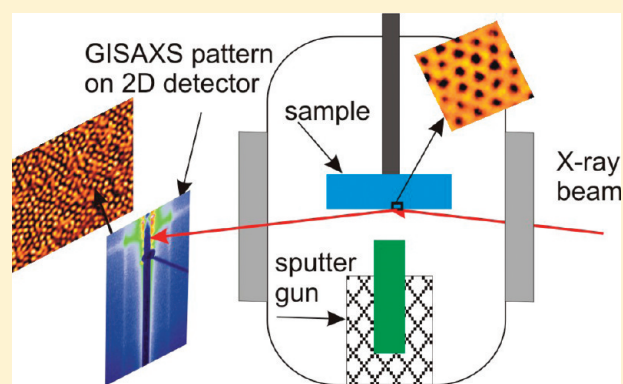
[†]Physik-Department E13, Lehrstuhl für Funktionelle Materialien, Technische Universität München, James-Franck Str. 1, 85748 Garching, Germany

[‡]HASYLAB at DESY, Notke Str. 85, Hamburg, Germany

[§]Martin-Luther-Universität Halle-Wittenberg, Von-Danckelmann-Platz 3, 06120 Halle, Germany

[⊥]Instituut voor Kern- en Stralingsfysica and INPAC, Celestijnenlaan 200D, K.U. Leuven, BE-3001 Leuven, Belgium

**ABSTRACT:** We investigate the formation of an ordered array of metal nanoclusters via selective doping of microphase-separated nanodomains in thin diblock copolymer films. Nanostructure formation during this doping process is probed *in situ* with microbeam grazing incidence small-angle X-ray scattering ($\mu$GISAXS) and *ex-situ* with atomic force microscopy (AFM). During sputter deposition of iron on the thin film template of polystyrene-*block*-poly(methyl methacrylate) P(S-*b*-MMA) copolymer, having upright cylindrical domains of PMMA, iron atoms selectively dope the PMMA domains due to the preferential chemical affinity. AFM confirms the $\mu$GISAXS results that the iron atoms preferentially wet the PMMA domains at low amount of sputter deposited iron. Up to a threshold of a nominal thickness of 2.0 nm deposited iron, the atoms wet only the PMMA domains and create the ordered array of metal nanoclusters. Above this threshold thickness the iron nanostructures grow laterally and finally cover the complete template surface.



## 1. INTRODUCTION

In general, miniaturization of devices demands functional materials on the nanoscale. In particular, ordered metal nanostructures are desirable to render the optical, electrical, magnetic, chemical, and biological properties in nanodevices.[1−15] On the basis of block copolymers, mesoscopic lattice structures can be produced through self-assembly.[16−22] The group of Russell[23] showed that 10 terabit per square inch domain density can be achieved with long-range lateral order in block copolymer thin films having upright cylindrical domain structures. Therefore, templates of such long-range hexagonal array of upright cylindrical domains, in a thin film of a block copolymer, can serve as advanced host materials for metal nanostructures.[1,24−32] So far, there have been several methods used to install metal nanostructures inside of the block copolymer domains. Among them, one common method is to remove the minor block from the film and refill the produced pores with the desired metallic materials.[18,19,33] The pores in the polymer films can be filled for example through vapor deposition of metal,[19] dip-coating from a nanoparticle dispersion,[34] and electrophoretic deposition.[35] Through particle cooperated self-assembly[1,24] colloidal nanoparticles can also be directed to the upright cylindrical domains present in block copolymer thin films. In this technique, the balance of the surface tension between the ligands of the nanoparticles and the interfacial tension between two blocks are responsible for a directional assembly of the nanoparticles

in a specific block. Physical vapor deposition and sputter deposition of noble metals on polymer surfaces and microphase-separated block copolymer templates[36−41] showed that the noble metals decorate one preferential block and form metal nanoparticles, metal wires, and chains of metal clusters depending on the used template morphology. Lopes et al. investigated selective wetting of metals on the copolymer polystyrene-*block*-poly(methyl methacrylate), denoted as P(S-*b*-MMA), having cylindrical domains parallel to the substrate and observed the formation of metal wires and clusters on the selective domains upon thermal evaporation of metal.[36,37] The selectivity was increased by further annealing above the glass transition temperature of the copolymer. However, the used thermal evaporation of metal leads to the formation of metal clusters on the polymer surface because of a very high surface free energy of the metal atoms produced by this preparation method. Therefore, metal nanodots having defined size and spacing may be achieved with only low energy metal deposition methods such as sputtering. So far, to our knowledge, selective doping of upright cylindrical domains in a block copolymer thin film by sputter deposition of ferromagnetic materials has not been reported.

In this article, we present a pathway to selectively deposit iron on a polymer film and thereby create ordered metal nanostructures. Our approach is based on the selective nature of doping of iron atoms during sputter deposition onto a thin film of the block copolymer P(S-*b*-MMA), having upright cylindrical domains of PMMA with lateral order. Such a thin film of P(S-*b*-MMA) is used as a template and iron ($^{57}$Fe) is sputtered on top of this template. Nanostructure formation and doping are investigated *in situ* with microbeam grazing incidence small-angle X-ray scattering ($\mu$GISAXS).[42] Additionally, the nanocomposites' surface morphology is investigated with atomic force microscopy (AFM) by using selected stages of iron surface coverage of the template.

## 2. EXPERIMENTAL SECTION

**Template Preparation.** An asymmetric diblock copolymer P(S-*b*-MMA) having a molecular weight of $M_W$ = 77 000 g/mol (molecular weight distribution $M_W/M_N$ = 1.09) and a random copolymer P(S-*r*-MMA) with $M_W$ = 31 100 g/mol (molecular weight distribution $M_W/M_N$ = 1.17) were purchased from Polymer Source Inc. The silicon (100) substrates were cleaned first with an acidic mixture of 160 mL of 96% sulfuric acid, 70 mL of 30% hydrogen peroxide, and 110 mL of deionized water at 80 °C, followed by a strong rinsing with deionized water.[43] The solution of the random copolymer of P(S-*r*-MMA) in toluene was spin-coated on top of clean silicon wafer pieces. The resulting thin film of P(S-*r*-MMA) on top of silicon was exposed to UV light for 30 min. During UV exposure, the double bonds present in PS broke and grafted on the silicon substrates. The excess polymers, which were not grafted, were removed from the substrate surface by subsequent washing with toluene. With a second spin-coating step a thin film of P(S-*b*-MMA) with a thickness of 81 nm was prepared from a solution of the polymer and toluene. The film was annealed at 165 °C and an oven under vacuum ($1 \times 10^{-3}$ mbar) conditions for 72 h. The treated diblock copolymer film has upright cylindrical domains of PMMA in a PS matrix.[1,44,45] In addition, three similar templates were prepared for AFM investigation by using HF acid-treated silicon substrates which are described in detail elsewhere.[1]

**Sputter Deposition of Iron.** We used a portable UHV system equipped with a dc magnetron sputtering source and two beryllium windows enabling simultaneous in-situ GISAXS experiments on the thin polymer film template during sputter deposition of iron.[41,46,47]

A schematic side view of the sputtering chamber used for this investigation is shown in Figure 1. The main chamber was pumped down by a two-stage turbomolecular pump to a base pressure lower than $5 \times 10^{-8}$ mbar. Argon (purity = 6.0) plasma was used to knock the iron atoms out of the target. The target was the iron isotope $^{57}$Fe (purity = 99.999%). Iron was sputtered at a pressure of $5 \times 10^{-3}$ mbar (argon pressure). At this pressure, no collisions of the iron atoms with the argon plasma is expected. The distance between the sample and the target was 6 cm. Iron was being sputter-deposited for 20 min with a rate of 0.2 nm/min for the *in situ* investigation. The sputter deposition rate was controlled with independent reference sample measurements. Along with the *in situ* $\mu$GISAXS study, three templates prepared by using HF treated silicon substrates were sputtered separately with 0.4, 0.8, and 2.0 nm nominal thicknesses of iron to investigate the change of the surface topography by AFM.

**Atomic Force Microscopy (AFM).** The surface topography of the template and the sputter-deposited templates were investigated by using an Autoprobe CP Research atomic force microscope in tapping mode. The measurements were performed at ambient conditions. We used gold-coated silicon cantilevers with a high aspect ratio (Ultralever cantilevers) having a resonance frequency of 60 kHz. Because of the high
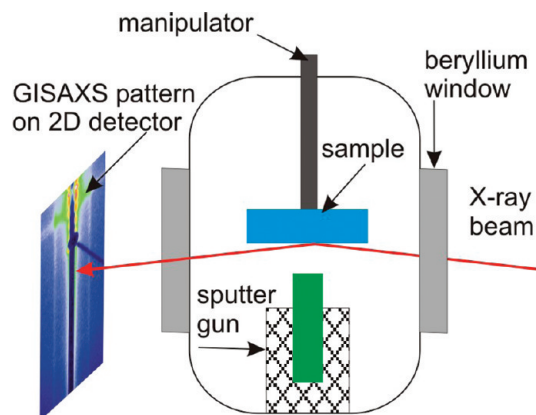


**Figure 1.** Schematic side view of the basic setup used in the *in situ* GISAXS experiment during sputter deposition. Two beryllium windows allow the X-ray beam to impinge on the sample mounted with the help of a manipulator and to collect the scattered intensity on the detector. The working pressure was $5 \times 10^{-3}$ mbar. The incident angle was $\alpha_i$ = 0.426°.

aspect ratio and an asymptotic conical shape, the polymer morphology was probed with a high lateral resolution. From the raw data, the background due to the scanner-tube movement was fully subtracted.

**Grazing Incidence Small-Angle X-ray Scattering (GISAXS).** The nanostructure formation during sputter deposition was investigated with *in situ* $\mu$GISAXS.[41,46] $\mu$GISAXS measurements were carried out at the beamline BW4 of the DORIS III storage ring at HASYLAB (DESY, Hamburg, Germany). During the $\mu$GISAXS measurements, the X-ray beam impinges on the thin film using an inverted geometry in comparison to the regular $\mu$GISAXS setup due to the geometry (see Figure 1) of the operated sputter deposition chamber. As a result, the measured 2d scattering pattern appeared on the detector inverted in the vertical direction in comparison with the standard $\mu$GISAXS geometry.[49] Two pointlike beam stops were used to block the direct and the specularly reflected beam in front of the detector to avoid damage of the detector. In addition, a third, rodlike movable beam stop was also used to block the very high intensity around $q_y = 0$ on the detector (see Figure 2b). The selected wavelength of the focused X-ray beam (beam size 60 $\mu$m $\times$ 30 $\mu$m) was $\lambda$ = 0.138 nm.[50] The incident angle was $\alpha_i$ = 0.426°, which is above the critical angles of PS (0.138°) and PMMA (0.146°). Therefore, the X-ray beam penetrates the whole film and the scattering data contains information on the structural lengths present in the full depth of the film. The distance between the sample and the detector was $D_{SD}$ = 1.96 m. A MARCCD detector was used to record the 2d scattering intensities every 60 s during sputtering. In total, 20 $\mu$GISAXS patterns were recorded.

## 3. RESULTS AND DISCUSSION

**a. Template Structures.** Figure 2a shows the phase image of the polymer template used for the presented investigation. Templates prepared by both methods, HF etching and coating with an ultrathin film of random copolymer, have similar morphology; i.e., the cylindrical domains of PMMA are oriented normal to the substrate surface in the PS matrix. Since the volume fraction of the PMMA block is 0.29, cylindrical domains of PMMA were formed due to microphase separation.[1,17,44,45] During annealing, these cylindrical domains of PMMA arranged themselves in a hexagonal array. Because the substrates are neutral, the cylindrical domains in P(S-*b*-MMA) block copolymer thin films orient predominantly perpendicular to the substrate surface.[50−54] Although the substrate is neutral to both blocks of the used P(S-*b*-MMA) copolymer, not all PMMA
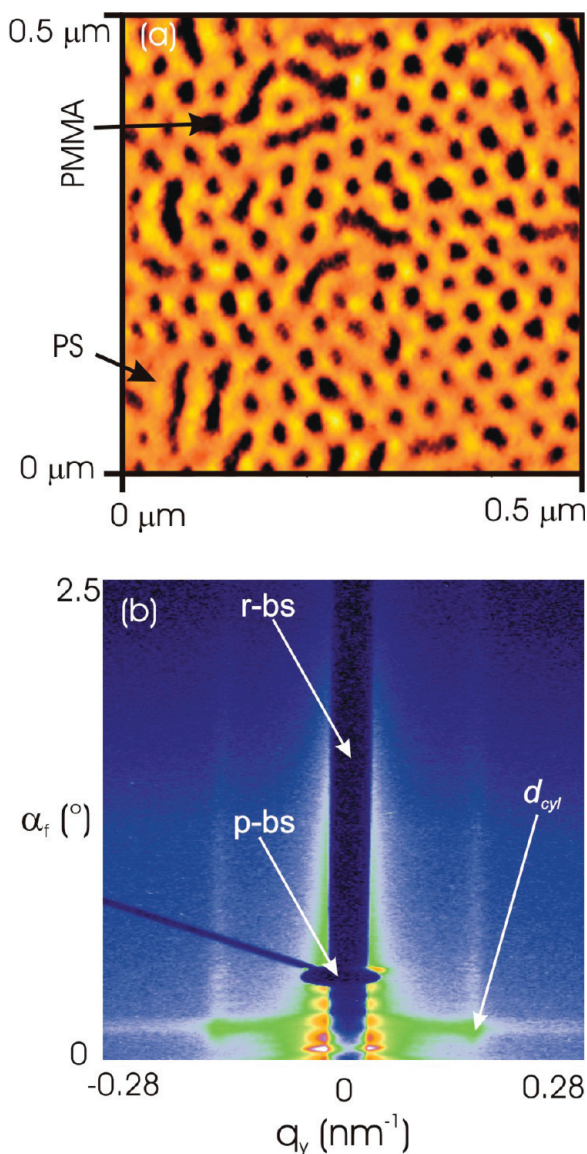
**Figure 2.** (a) Atomic force microscopic phase image of the template used for sputter deposition of iron. The phase images show the presence of upright cylindrical domains of PMMA (dark spots) in PS matrix (yellowish phase). (b) $\mu$GISAXS pattern of the pure template on 2d detector. The side intensity maxima represent the average cylinder-to-cylinder distance, $d_{cyl}$. p-bs and r-bs stand for point-beamstop and rod-beamstop, respectively.

domains are perfectly oriented normal to the substrate, but few domains of PMMA are randomly oriented. The film surface is very smooth with a rms roughness of only 0.2 nm. Islands or holes, which are typical for microphase-separated block copolymer film, are not observed in the AFM investigation. Because of the presence of the neutral substrate, the whole film wets the substrate completely and contains upright cylindrical domains of PMMA, as described above. The average diameter of the cylinders, $D_{cyl}$, and the cylinder-to-cylinder distance, $d_{cyl}$, measured by AFM image processing software IP 2.1, are $27 \pm 3$ nm and $45 \pm 3$ nm, respectively. The corresponding $\mu$GISAXS data of the template shows one side maximum at a position of $q_y = 13.6 \times 10^{-2}$ nm$^{-1}$ (see Figure 2b), which originates from the cylinder-to-cylinder distance of $46 \pm 1$ nm. Thus, we find good

agreement between the structures observed in AFM and $\mu$GI-SAXS, demonstrating that the AFM data shown are well representative for the sample under investigation. The reason for the absence of more pronounced intensity side maxima (higher intensity in first orders) is that the electron density difference between the PS and the PMMA phases is not very high. The absence of higher order maxima is caused by the deviations from a perfect hexagonal arrangement of the cylinders as seen by the AFM as well.

**b. Template Doping with Iron by Sputter deposition: An in Situ GISAXS Study.** The P(S-b-MMA) block copolymer thin film template is mounted on the sample holder with the surface of the film facing down toward the metal source as shown in Figure 1. Because of the presence of two beryllium windows along the flight path of the incoming and scattered X-ray beam, in situ $\mu$GISAXS measurements are feasible during sputter deposition. Figure 3 shows three selected $\mu$GISAXS data and the corresponding simulated scattering patterns using the IsGISAXS software.[55] The principal features of all scattering patterns are the pronounced intensity side maxima which are already present in the pure template. The intensity of these side maxima is noticeably changing with increasing amount of sputter deposited iron. However, the position of the intensity side maxima remains constant at $q_y = 13.6 \times 10^{-2}$ nm$^{-1}$. Moreover, the intensity of the side maxima increases without any distinguishable diffuse intensity around each side maximum, up to 2.0 nm of iron sputter deposition (nominal thickness). The appearance of these intensity side maxima is due to an increase of electron density contrast among the nanostructures present in the film with a regular lateral distance and shape of the structures upon sputter deposition. The sputter-deposited iron creates this electron density difference between the cylindrical domains of PMMA and the matrix PS. This indicates that the sputtered iron atoms selectively wet or adsorb to one of the blocks in the P(S-b-MMA) diblock copolymer film template. Either the iron atoms stick preferentially to only one domain or they diffuse inside the film and dewet preferentially from one domain and migrate toward the other domain. However, only from the scattering data it is difficult to conclude which domain the iron atoms preferentially wet.

To extract the structural information from the $\mu$GISAXS data, we simulated all the 2d scattering patterns assuming a very simple model of our system using the IsGISAXS[55] software. In this simple model, we assumed our template to be a thin polymer film of constant electron density on top of a silicon substrate, and the iron nanostructures grow vertically and laterally on top of the film. The scattered intensities have been calculated according to the distorted-wave Born approximation (DWBA).[56] Three examples of simulated 2d $\mu$GISAXS patterns are given in Figure 3 (a′, b′, and c′). These are $\mu$GISAXS patterns after sputter deposition of 0.4, 0.8, and 2.0 nm of nominal height of iron. The structural information is extracted from the data and the simulation. To better show the evolution during sputtering, the off-detector cuts[42,57,58] at the position of one side intensity maximum and the structural change due to sputter deposition of iron are shown in Figure 4.

The vertical intensity modulation in the off-detector cuts becomes stronger with increasing amount of sputtered iron (see Figure 4a). In addition, the position of the intensity maximum in the off-detector cuts changes, and a second intensity maximum appears with increasing height of sputtered iron (shown by arrows in Figure 4a). This is a clear indication of the vertical growth of the
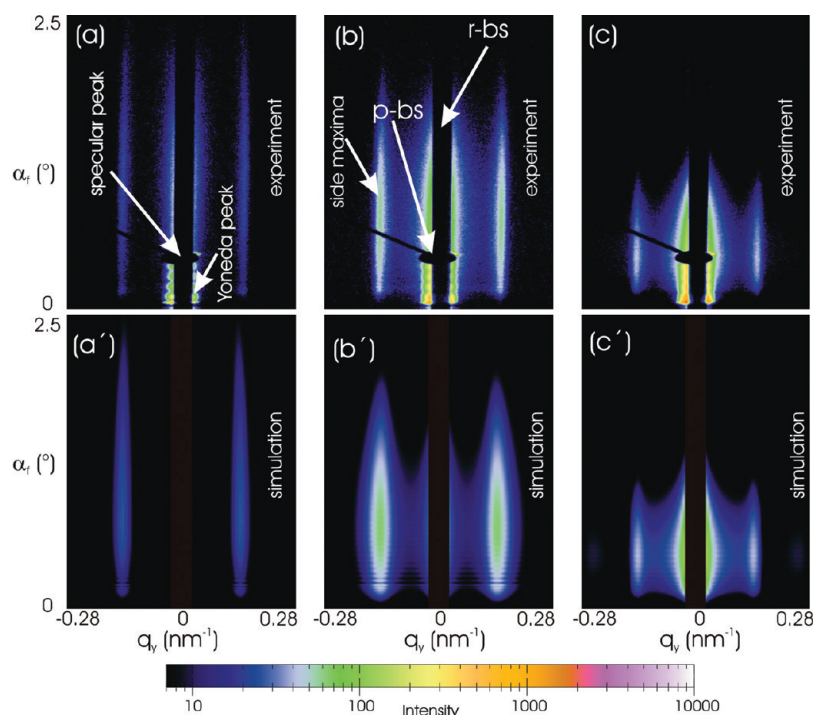
**Figure 3.** 2d $\mu$GISAXS patterns originating from the sample after sputter deposition of 0.4 nm (a, a′), 0.8 nm (b, b′), and 3.8 nm (c, c′) of nominal thickness of iron. (a), (b), and (c) are the data and (a′), (b′), and (c′) are the simulations using the IsGISAXS[55] software. The logarithmic color scale is selected for better contrast among the present features. A rod-beamstop (r-bs) and a point-beamstop (p-bs) were used to protect the detector from very high intensity of the reflected X-ray beam. The intensity of the side maxima increases with the amount of sputter-deposited iron.
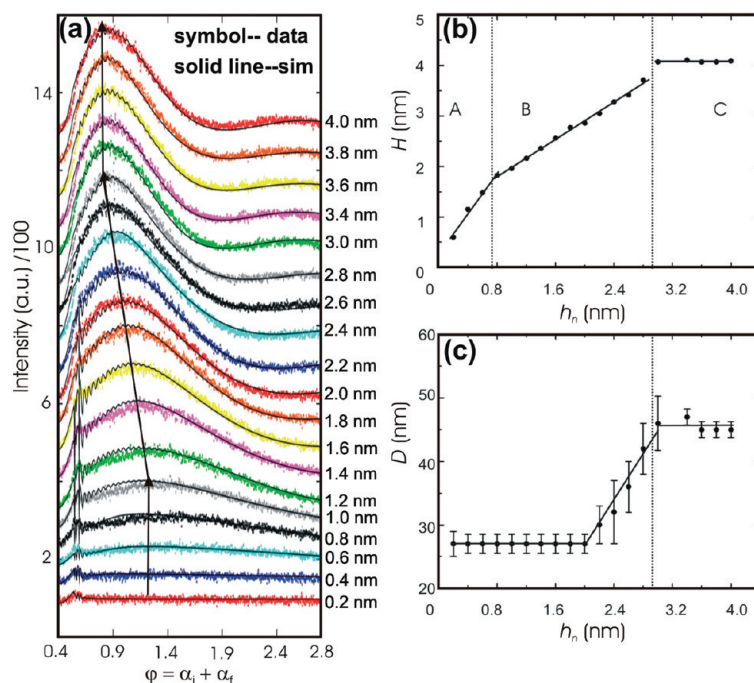


**Figure 4.** (a) Intensities of the off-detector cuts of the data and the corresponding fits from the simulations with IsGISAXS are plotted as a function of $\varphi = \alpha_i + \alpha_f$, where $\alpha_i$ is the incident angle of the X-ray beam on the sample and the $\alpha_f$ is the exit angle of the scattered beam. The symbols are the data and the solid lines are the simulation. The curves are shifted vertically against each other for better presentation. The nominal heights of the sputter-deposited iron are shown on the right to the corresponding curves. (b) Extracted object heights, denoted by $H$, of the nanostructures are plotted as a function of the nominal height, $h_n$. A, B, and C indicate three regimes with different growth rates. The solid lines are the linear fits. (c) The object diameters $D$ of the nanostructures are plotted as a function of $h_n$.

nanostructures. To understand the growth kinetics, the heights of the nanostructures, extracted from the simulations, are plotted

in Figure 4b. Three regimes with different growth rates, relative to the sputtering rate, are observed, which are marked as A, B, and

C in Figure 4b. Up to a height of 0.8 nm the growth rate is 0.45 nm/min, whereas the sputtering rate is 0.2 nm/min; i.e., the growth rate at the initial stage (A) is 2.25 times higher than the sputtering rate. The growth rate at the intermediate stage (B) is 0.18 nm/min, which is 0.9 times the sputtering rate. It seems that the growth rate is almost equal to the sputtering rate at this stage. The growth of the height stops when the height reaches ~4 nm. Afterward, the height remains constant, and no vertical growth is observed until the end of the *in situ* sputtering experiment. The diameter of the nanostructures shows also significant changes with the nominal height of the sputtered iron. As well, we observe three different regimes of object size growth (diameters). From the start until 2.0 nm of nominal height of sputtered iron the diameter remains almost constant at a value of $27 \pm 1.5$ nm, which is almost equal to the diameter of the PMMA cylinders present in the template. So, it seems that the iron atoms prefer to wet the PMMA blocks. With increasing amount (above 2 nm of nominal height of sputtered iron) of iron, the diameter increases linearly up to $47 \pm 2$ nm and then remains constant until the end of the experiment. Since the cylinder-to-cylinder distances present in the template are $46 \pm 1$ nm (obtained by simulation), it can be assumed that the iron atoms start to diffuse to the PS matrix or the nanostructures grow laterally on the PS matrix above a threshold (2 nm) of nominal amount of sputtered iron. The lateral growth stops after sputter deposition of iron with 3 nm of nominal amount, and they merge to cover the whole surface of the template. Since no vertical and lateral growth of the nanostructures on top of the template is observed at this stage, it can be assumed that the rest of sputter-deposited iron atoms diffuses into the template.

This *in situ* $\mu$GISAXS investigation shows that in the early stages below a critical amount of sputter deposited iron, the iron nanostructures reproduce the polymer film morphology, having both, the diameter and lattice spacing similar to the diameter and lattice spacing present in the template. Therefore, the polymer film acts as a perfect template in this regime. This leads us to the assumption that the iron atoms selectively dope PMMA domains below a critical amount of sputtered iron (2 nm) for the applied experimental conditions. The exact value of this critical amount may vary for different template structures and depend on the template sample temperature as well as the sputtering conditions (deposition rate, etc.). At a higher sputter deposition rate this critical amount can decrease and at a slower deposition rate it can increase, respectively. Moreover, a better selectivity may be achieved at slower deposition rate. In addition, the size of the available PMMA domains will play an important role as well. The larger the open area of the PMMA domains is, the more effective the iron deposition is to be expected. However, to detail the dependence of the critical amount on all these parameters goes beyond the scope of this investigation. To confirm the assumption of domain doping, we prepared three more block copolymer film templates, sputtered with different amounts of iron onto them, and investigated the resulting samples *ex situ* with AFM.

**c. Iron-Doped PMMA Phase: AFM Investigation.** Three templates with a very similar surface morphology, having upright cylindrical domains of PMMA in a PS matrix, are used in an *ex situ* AFM investigation of the surface morphology. On these templates iron of different nominal thicknesses is sputtered using identical sputter deposition conditions as we had applied in the *in situ* experiment. The selected nominal iron thicknesses are comparable to those in the *in situ* $\mu$GISAXS study. To focus on
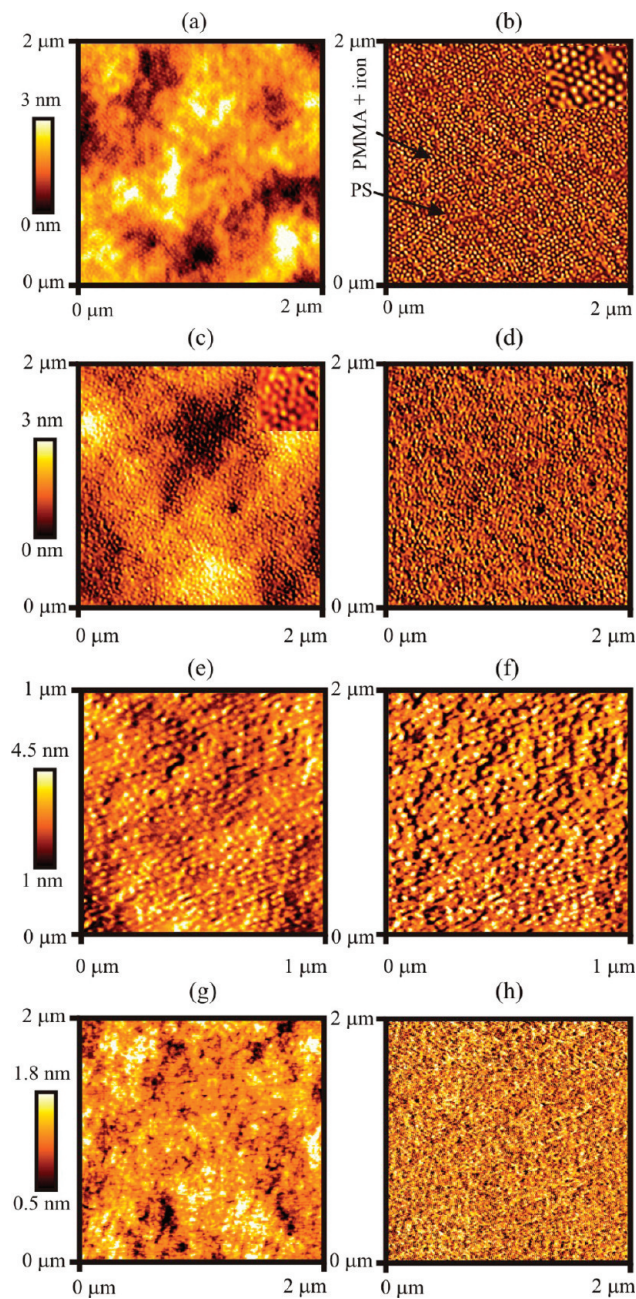


**Figure 5.** Topography (a, c, e, g) and phase (b, d, f, h) images of the template obtained by AFM investigation after sputter deposition of iron with nominal amount of 0.4 nm (a, b), 0.8 nm (c, d), 2.0 nm (e, f), and 4.0 nm (g, h). The presence of nanostructures formed by sputter deposition of iron can be observed in both topography and phase images as the bright spots in a yellowish matrix of PS in (a−f). The inset shows clearly the iron-doped PMMA domains.

the initial stages, all three nominal thickness values are chosen to be smaller than the critical limit of doping of the PMMA domains, as probed with $\mu$GISAXS.

Figure 5 shows the surface topography as probed with AFM and the corresponding phase images of the templates after sputter deposition of the iron with different nominal amounts (0.4, 0.8, and 2.0 nm). For comparison, the sample prepared in the *in situ* sputter experiment is shown as well (nominal amount 4.0 nm). The topography images (a, c, and e) show the presence of nanostructures of iron on top of the PMMA domains. If we

compare the phase images of the iron-sputtered templates shown in Figure 5b,d,f with the pure template shown in Figure 2a, we can see a strong phase contrast being generated because of the presence of the hard iron atoms on top of the relatively softer PMMA domains. The dark PMMA spots become brighter than the PS matrix because of the presence of iron. Besides, the height of the nanostructures increases with the increased amount of sputtered iron. If the iron atoms had decorated preferentially inside the PS matrix at the early stage of sputter deposition, we would be able to see the generation of a layer of iron with holes in the AFM investigation. No aggregate or cluster of iron has been observed on top of the PS matrix. Therefore, combining the findings of the *in situ* $\mu$GISAXS and AFM investigation, we confirm the selective doping of PMMA by the iron atoms below a critical limit of sputter deposition.

After the *in situ* $\mu$GISAXS investigation, the sample was investigated with AFM as well. The corresponding topography and phase images are shown in Figure 5g,h. Neither a nanostructure has been found on top of the template, nor a phase contrast has been seen in the phase image. Only a flat surface was probed. This leads us to the conclusion that the whole template is fully covered with iron atoms after sputter deposition of iron with a nominal amount of 4 nm. This fully agrees with the findings of the *in situ* $\mu$GISAXS study already mentioned before.

The question is, why are the iron atoms selectively decorating PMMA at the early stage of sputter deposition? The possible answer is in the chemical interaction between the polymer blocks of the diblock copolymer and the iron atoms. PMMA has a polar carbonyl group as a side chain. A carbonyl group has a partially negatively charged oxygen atom due to the strong electronegative nature of the oxygen atom. Iron atoms are nucleophilic in nature due to the shortage of two electrons in the 3d orbital. As a result, the negatively charged oxygen atoms attract the nucleophilic iron atoms, leading to selective doping of the PMMA cylindrical domains by the iron atoms. In thin films of polymer, a large amount of free volume is present due to the rotational and translational entropy of the polymer chains during the film formation. The iron atoms can diffuse easily through the PS phase of the film and migrate toward the PMMA phase at the early stage of sputter deposition (region A in Figure 4b). The driving force of this migration of iron atoms is assumed to be polar interaction. When the top surface of the PMMA domains is saturated with iron atoms, the subsequently sputtered atoms can no longer be accommodated in the PMMA domains. As a result, the deposition and diffusion of the iron atoms toward the PMMA domains extend inside the PS phase, which causes an increase of diameters of the formed nanostructures that can be observed at the intermediate stage of sputter deposition (regime B in Figure 4b). It is to be expected that a larger open area of the PMMA domains (for example, in a lamellar diblock copolymer system) would increase the probability of selective deposition and prevent the diffusion of iron atoms to the PS at this stage.

## 4. CONCLUSION

We have successfully investigated the selective nature of metal doping during sputter deposition of iron on a P(S-*b*-MMA) diblock copolymer film template having upright cylindrical domains of PMMA in a PS matrix. Both, real-space and reciprocal-space characterization techniques have been used complementarily to investigate this iron deposition. *Ex situ* AFM maps the surface topography. $\mu$GISAXS probes the inner film structure

in addition. The *in situ* $\mu$GISAXS investigation allows for the detection of the critical nominal thickness of iron (2.0 nm) maintaining the region of selective block doping. Below this critical nominal thickness, sputter-deposited iron atoms selectively wet the PMMA domains only. On the one hand, iron atoms can act as a nucleophilic agent. On the other hand, carbonyl groups present in the side chain of PMMA have a highly electronegative oxygen. As a result, the interaction between the nucleophilic iron atoms and partially negatively charged oxygen atoms of carbonyl groups drives iron atoms to deposit preferentially on the PMMA domains. Above the critical limit, the nanostructures grow laterally and cover the whole template surface. Thus, preferential doping of PMMA domains by iron opens a new route to create ordered metallic nanostructures with a controlled size in terms of regular distance and diameter by using microphase-separated block copolymer thin film templates.

To extend the observed behavior to other polymer template and metal systems might however not be that easy. On the one hand, the creation of polymer templates with upright cylinder structures so far only worked for a limited number of diblock copolymer systems. On the other hand, the selective interaction of the metal atoms with one of the blocks from the diblock copolymer is of major importance to prevent a continuous metal decoration of the surface. Moreover, the sputter deposition has to be performed in a gentle manner to prevent a distortion of the polymer template by the deposited metal.

## ■ AUTHOR INFORMATION

### Corresponding Author
*Phone +498928912451, fax +498928912473; e-mail muellerb@ph.tum.de (P.M.-B.), mottakin.abul.kashem@desy.de (M.M.A.K.).

## ■ REFERENCES

(1) Abul Kashem, M. M.; Perlich, J.; Diethert, A.; Wang, W.; Memesa, M.; Gutmann, J.; Majkova, E.; Capek, I.; Roth, S. V.; Petry, W.; Müller-Buschbaum, P. *Macromolecules* **2009**, *42*, 6202.

(2) Warren, S. C.; Messina, L. C.; Slaughter, L. S.; Kamperman, M.; Zhou, Q.; Gruner, S. M.; Disalvo, F. J.; Wiesner, U. *Science* **2008**, *320*, 1748.

(3) Ghosh, P. S.; Kim, C.-K.; Han, G.; Forbes, N. S.; Rotello, V. M. *ACS Nano* **2008**, *2*, 2213.

(4) Balazs, A. C.; Emrick, T.; Russell, T. P. *Science* **2006**, *314*, 1107.

(5) Lenz, S.; Nett, S. K.; Memesa, M.; Roskamp, R. F.; Timmann, A.; Roth, S. V.; Berger, R.; Gutmann, J. S. *Macromolecules* **2010**, *43*, 1108.

(6) Bajaj, A.; Miranda, O. R.; Phillips, R.; Kim, I.-B.; Jerry, D. J.; Bunz, U. H. F.; Rotello, V. M. *J. Am. Chem. Soc.* **2010**, *132*, 1018.

(7) Daniel, M.-C.; Tsvetkova, I. B.; Quinkert, Z. T.; Murali, A.; De, M.; Rotello, V. M.; Kao, C. C.; Dragnea, B. *ACS Nano* **2010**, *4*, 3853.

(8) Mann, S.; Ozin, G. A. *Nature* **1996**, *382*, 313.

(9) Abul Kashem, M. M.; Perlich, J.; Schulz, L.; Roth, S. V.; Petry, W.; Müller-Buschbaum, P. *Macromolecules* **2007**, *40*, 5075.

(10) Darling, S. B.; Yufa, N. A.; Cisse, A. L.; Bader, S. D.; Sibener, S. J. *Adv. Mater.* **2005**, *17*, 2446.

(11) Lauter-Pasyuk, V.; Lauter, H. J.; Gordeev, G. P.; Müller-Buschbaum, P.; Toperverg, B. P.; Petry, W.; Jernenkov, M.; Petrenko, A.; Aksenov, V. *Physica B* **2004**, *350*, e939.

(12) Roth, S. V.; Walter, H.; Burghammer, M.; Riekel, C.; Lengeler, B.; Schroer, C.; Kuhlmann, M.; Walther, T.; Sehrbrock, A.; Domnick, R.; Müller-Buschbaum, P. *Appl. Phys. Lett.* **2006**, *88*, 021910.

(13) Perlich, J.; Kaune, G.; Memesa, M.; Gutmann, J. S.; Müller-Buschbaum, P. *Philos. Trans. R. Soc., A* **2009**, *367*, 1783.

(14) Warren, S. C.; Wiesner, U. *Pure Appl. Chem.* **2009**, *81*, 73.

(15) Nedelcu, M.; Lee, J.; Crossland, E. J. W.; Warren, S. C.; Orilall, M. C.; Guldin, S.; Huettner, S.; Ducati, C.; Eder, D.; Wiesner, U.; Steiner, U.; Snaith, H. J. *Soft Matter* **2009**, *5*, 134.

(16) Lee, B.; Park, I.; Yoon, J.; Park, S.; Kim, J.; Kim, K. W.; Chang, T.; Ree, M. *Macromolecules* **2005**, *33*, 3250.

(17) Park, H. W.; Im, K.; Chung, B.; Ree, M.; Chang, T.; Sawa, K.; Jinnai, H. *Macromolecules* **2007**, *40*, 2603.

(18) Kim, S. H.; Misner, M. J.; Xu, T.; Kimura, M.; Russell, T. P. *Adv. Mater.* **2004**, *16*, 226.

(19) Park, S.; Wang, J.-Y.; Kim, B.; Xu, J.; Russell, T. P. *ACS Nano* **2008**, *2*, 766.

(20) Yoon, J.; Jin, S.; Ahn, B.; Rho, Y.; Hirai, T.; Maede, R.; Hayakawa, T.; Kim, J.; Kim, K. W.; Ree, M. *Macromolecules* **2008**, *41*, 8778.

(21) Bosworth, J. K.; Marvin, P. Y.; Ricardo, R.; Schwartz, E. L.; Huang, J. Q.; Ko, A. W.; Smilgies, D.-M.; Black, C. T.; Ober, C. K. *ACS Nano* **2008**, *2*, 1396.

(22) Dobriyal, P.; Xiang, H.; Kazuyuki, M.; Chen, J.-T.; Jinnai, H.; Russell, T. P. *Macromolecules* **2009**, *42*, 9082.

(23) Park, S.; Lee, D. H.; Xu, J.; Kim, B.; Hong, S. W.; Jeong, U.; Xu, T.; Russell, T. P. *Science* **2009**, *323*, 1030.

(24) Lin, Y.; Böker, A.; He, J.; Sill, K.; Xiang, H.; Abetz, C.; Li, X.; Wang, J.; Emrick, T.; Lung, S.; Wang, Q.; Balazs, A.; Russell, T. P. *Nature* **2005**, *434*, 55.

(25) Kim, H.-C.; Jia, X.; Stafford, C. M.; Kim, D. H.; McCarthy, T. J.; Tuominen, M.; Hawker, C. J.; Russell, T. P. *Adv. Mater.* **2001**, *13*, 795.

(26) Aleksandrovic, V.; Greshnykh, D.; Randjelovic, I.; Frömsdorf, A.; Kornowski, A.; Roth, S. V.; Klinke, C.; Weller, H. *ACS Nano* **2008**, *2*, 1123.

(27) Park, S.-M.; Craig, G. S. W.; Liu, C.-C.; La, Y.-H.; Ferrier, N. J.; Nealey, P. F. *Macromolecules* **2008**, *41*, 9118.

(28) Thompson, R. B.; Ginzburg, V. V.; Matson, M. W.; Balazs, A. C. *Science* **2001**, *292*, 2469.

(29) Huh, J.; Ginzburg, V. V.; Balazs, A. C. *Macromolecules* **2000**, *33*, 8085.

(30) Gowd, E. B.; Nandan, B.; Bigall, N. C.; Eychmuller, A.; Formanek, P.; Stamm, M. *Polymer* **2010**, *51*, 2661.

(31) Gowd, E. B.; Nandan, B.; Vyas, M. K.; Bigall, N. C.; Eychmuller, A.; Schlorb, H.; Stamm, M. *Nanotechnology* **2009**, *20*, 415302.

(32) Thompson, R. B.; Ginzburg, V. V.; Matson, M. W.; Balazs, A. C. *Macromolecules* **2000**, *35*, 1060.

(33) Darling, S. B. *Surf. Sci.* **2007**, *601*, 2555.

(34) Misner, M. J.; Skaff, H.; Emrick, T.; Russell, T. P. *Adv. Mater.* **2003**, *15*, 221.

(35) Zhang, Q.; Xu, T.; Butterfield, D.; Misner, M. J.; Ryu, D. Y.; Emrick, T.; Russell, T. P. *Nano Lett.* **2005**, *5*, 357.

(36) Lopes, W. A.; Jaeger, H. M. *Nature* **2001**, *414*, 735.

(37) Lopes, W. A. *Phys. Rev. E* **65**, 031606.

(38) Faupel, F.; Zaporojtchenko, V.; Strunskus, T.; Greve, H.; Schurmann, U.; Takele, H.; Hanisch, C.; Chakravadhanula, V. S. K.; Ni, N.; Gerber, A.; Quandt, E.; Podschun, R. *Polym. Polym. Compos.* **2008**, *16*, 471.

(39) Takele, H.; Jebril, S.; Strunkus, T.; Zaporojchenko, V.; Adelung, R.; Faupel, F. *Appl. Phys. A: Mater. Sci. Process.* **2008**, *92*, 345.

(40) Beyene, H. T.; Chakravadhanula, V. S. K.; Hanisch, C.; Elbahri, M.; Strunskus, T.; Zaporojtchenko, V.; Kienle, L.; Faupel, F. *J. Mater. Sci.* **2010**, *45*, 5865.

(41) Metwalli, E.; Couet, S.; Schlage, K.; Röhlsberger, R.; Körstgens, V.; Ruderer, M.; Wang, W.; Kaune, G.; Roth, S. V.; Müller-Buschbaum, P. *Langmuir* **2008**, *24*, 4265.

(42) Müller-Buschbaum, P. *Anal. Bioanal. Chem.* **2003**, *376*, 3.

(43) Müller-Buschbaum, P. *Eur. Phys. J. E* **2003**, *12*, 443.

(44) Kang, G. B.; Kim, S.-I.; Kim, Y. T.; Park, J. H. *Curr. Appl. Phys.* **2009**, *9*, S82.

(45) Xu, T.; Kim, H.-C.; DeRouchey, J.; Seney, C.; Levesque, C.; Martin, P.; Stafford, C. M.; Russell, T. P. *Polymer* **2001**, *42*, 9091.

(46) Diederich, T.; Couet, S.; Röhlsberger, R. *Phys. Rev. B* **2007**, *76*, 054401.

(47) Couet, S.; Diederich, T.; Schlage, K.; Röhlsberger, R. *Rev. Sci. Instrum.* **2008**, *79*, 093908.

(48) Kaune, G.; Ruderer, M. A.; Metwalli, E.; Wang, W.; Couet, S.; Schlage, K.; Röhlsberger, R.; Roth, S. V.; Müller-Buschbaum, P. *ACS Appl. Mater. Interfaces* **2009**, *1*, 353.

(49) Roth, S. V.; Dohrmann, R.; Dommach, M.; Kuhlmann, M.; Kroger, I.; Gehrke, R.; Walter, H.; Schroer, C.; Lengeler, B.; Müller-Buschbaum, P. *Rev. Sci. Instrum.* **2006**, *77*, 085106.

(50) Kellog, G. J.; Walton, D. G.; Mayes, A. M.; Lambooy, P.; Russell, T. P.; Galagher, P. D.; Satija, S. K. *Phys. Rev. Lett.* **1996**, *76*, 2503.

(51) Mansky, P.; Russell, T. P.; Hawker, C. J.; Pitsikalis, M.; Mays, J. *Macromolecules* **1997**, *30*, 6810.

(52) Mansky, P.; Liu, Y.; Huang., E.; Russell, T. P.; Hawker, C. *Science* **1997**, *274*, 1458.

(53) Peters, P. D.; Yang, X. M.; Kim, T. K.; Nealey, P. F. *Langmuir* **2000**, *16*, 9620.

(54) Potemkin, I. I. *Macromolecules* **2004**, *37*, 3504.

(55) Lazzari, R. R. *Appl. Crystallogr.* **2002**, *35*, 406.

(56) Sinha, S. K.; Sirota, E. B.; Garoff, S.; Stanley, H. B. *Phys. Rev. B* **1998**, *38*, 2297.

(57) Salditt, T.; Metzger, T. H.; Peisl, J.; Reinker, B.; Moske, M.; Samwer, K. *Europhys. Lett.* **1995**, *32*, 331.

(58) Salditt, T.; Metzger, T. H.; Peisl, J.; Goerigk, G. *J. Phys. D: Appl. Phys.* **1995**, *28*, A236.